Prepared for submission to JINST

FERMILAB-PUB-16-656-AD-CD-TD
ACCEPTED

Muon Counting using Silicon Photomultipliers in the AMIGA detector of the Pierre Auger Observatory

The Pierre Auger collaboration

E-mail: auger_spokespersons@fnal.gov

Abstract: AMIGA (Auger Muons and Infill for the Ground Array) is an upgrade of the Pierre Auger Observatory designed to extend its energy range of detection and to directly measure the muon content of the cosmic ray primary particle showers. The array will be formed by an infill of surface water-Cherenkov detectors associated with buried scintillation counters employed for muon counting. Each counter is composed of three scintillation modules, with a $10\,m^2$ detection area per module. In this paper, a new generation of detectors, replacing the current multi-pixel photomultiplier tube (PMT) with silicon photo sensors (aka. SiPMs), is proposed. The selection of the new device and its front-end electronics is explained. A method to calibrate the counting system that ensures the performance of the detector is detailed. This method has the advantage of being able to be carried out in a remote place such as the one where the detectors are deployed. High efficiency results, i.e. efficiency 96 % for the higher tested overvoltage, combined with a low probability of accidental counting (~2 %), show a promising performance for this new system.

Keywords: Muon detector; SiPM; Photomultiplier; Front-end electronics; Calibration method

Operated by Fermi Research Alliance, LLC under Contract No. DE-AC02-07CH11359 with the United States Department of Energy.

Contents

1 Introduction

The Pierre Auger Obsevatory [1] is located in the province of Mendoza, Argentina and has an area of 3000 km^2. It was designed to detect ultra-high energy cosmic ray showers with a hybrid detection technique. It has 1660 surface water-Cherenkov detector stations (SDs) [2] arranged in a triangular grid, with a distance of ~1.5 km between stations, and 27 fluorescence detector (FD) telescopes [3] at four sites on the periphery of the array, pointing towards the atmosphere and the center of the array. The Auger Observatory is currently being upgraded, and AMIGA [4–6] (Auger Muons and Infill for the Ground Array) is one of the principal enhancements. Two of the main objectives of AMIGA are the measurement of composition-sensitive observables of extensive air showers and the study of features of hadronic interactions. Important results on cosmic ray physics by means of the muon detection techniques have been previously obtained by several experiments like KASCADE [7] and KASCADE-Grande [8].

AMIGA consists of 61 detector pairs, each one composed of a SD station and a 30 m^2 muon counter, deployed on a 750 m triangular grid in an infilled area of 23.5 km^2. Each muon counter is buried underground to shield the electromagnetic component of cosmic ray showers and it is composed of three scintillation modules. Every module comprises 64 scintillation bars, each of dimensions 400 cm x 4 cm x 1 cm, with a 1.2 mm diameter wavelength-shifting (WLS) optical fiber glued to a lengthwise groove on each bar. The light produced in the bars is absorbed by the WLS fiber. The excited molecules of the fiber decay while emitting photons, some of which are propagated along the WLS fibers towards a channel of a multi-pixel photon detector. The aim of these modules is to count efficiently the number of muons that impinge on the 10 m^2 area of scintillation [9].

A new generation of detectors is being developed to replace current multi-pixel photomultiplier tubes (PMTs) with silicon photo sensors (aka. SiPMs). The main advantages of these devices, compared to current PMTs, are their lower cost per channel, a better definition of the signal produced by the impinging photon, longer life-time, better sturdiness, higher photon detection efficiency at the optical fiber emission wavelength, and no optical cross-talk between channels. All these advantages motivate the proposal of a new counting system.

The present paper is organized in the following way: a general description of the SiPM behaviour is detailed in section 2. Then the SiPM and the front-end electronics selection is explained in section 3. The proposed calibration of the counting system is described in section 4. Finally, the efficiency measurements are shown in section 5.

2 The Silicon Photomultiplier

A SiPM [10] is a solid-state device capable of detecting individual photons. It is composed of an array of cells, all connected in parallel. Each cell has an avalanche photo-diode (APD) working in Geiger mode and a quenching resistor (R_Q) in series (see figure 1).

The APD starts working in Geiger mode when the reverse voltage (V_{bias}) applied to it exceeds a specific voltage value called the breakdown voltage (V_{BR}). In this mode the injection of a single charge carrier (e.g. due to an impinging photon) causes a self-sustained avalanche. The current that flows through the APD depends on the voltage value over the breakdown which is called

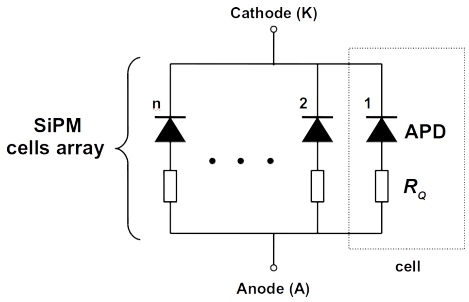

Figure 1. Schematic view of the internal structure of a SiPM made up of an array of cells, all connected in parallel. Each cell is composed of an APD working in Geiger mode and a quenching resistor (R_Q) in series.

overvoltage ($\Delta V = V_{bias} - V_{BR}$). The flow of this current through R_Q produces the decrease of the reverse voltage (V_{APD}) applied to the APD. When V_{APD} is below V_{BR} the avalanche is extinguished. This last sequence describes the "firing" of a cell. From now on, the signal produced by this firing process will be called *single photon equivalent* (SPE). If multiple cells are fired simultaneously the resulting output signal will be a superposition of SPEs. The amplitude of this signal will be directly proportional to the number of fired cells. The total charge produced in the avalanche can be calculated with equation 2.1 and the gain (M) of this process is defined by equation 2.2.

$$Q = C_j \Delta V \tag{2.1}$$

$$M = Q/e \quad \text{where } e \text{ is the electron charge.} \tag{2.2}$$

It can be inferred from equations 2.1 and 2.2 that the gain depends linearly on the overvoltage. Therefore for the special case when the gain is zero, $V_{bias} = V_{BR}$. This equivalence will be important for the calibration procedure.

As was previously mentioned, SiPMs are employed to detect photons. An undesirable effect is the accidental counting of those photons due to noise in the cells. In the next subsection, the sources of noise are defined.

2.1 SiPM Noise

Noise in SiPMs [11] is defined as the firing of a cell that was not produced by a photon impinging the device. There are three noise sources which can be separated in two types, depending on the correlation or not with the firing of a cell.

2.1.1 Uncorrelated Noise: Dark Noise

Dark noise occurs randomly due to the thermally-generated charge carriers (electron-hole pairs) either in the depletion region or in the avalanche region [12]. The amplitude and shape of these pulses are the same as the ones produced by the absorption of a photon. Dark noise is sensitive to the temperature, and also depends on the array of cells size, overvoltage magnitude, and semiconductor material quality.

2.1.2 Correlated Noise: Afterpulsing and Cross-Talk

- Afterpulsing is a secondary avalanche produced after the firing of a cell, due to the release of trapped charges. The release of these trapped charges occurs after a characteristic time that depends on the type of the trapping centers and its occurrence probability decreases exponentially with time. It is noise correlated to the firing of a cell and it is produced in the same cell.

- When a primary avalanche in a cell produces photons with energy greater than the band gap energy, there is a probability that a nearby cell absorbs the photon, producing its firing. The secondary avalanche is in first order synchronized in time to the main primary avalanche to produce a resulting signal of a channel with an increased amount of SPEs stacked. This effect is called cross-talk.

3 Proposed Readout for AMIGA Muon Counters

The proposed electronics of the module must facilitate the identification of pulses above a given threshold to allow muon counting, without knowing in detail the signal structure and peak intensity.

Based on simulations [13], each of the three scintillator modules of a muon counter is segmented into 64 segments. The detector segmentation is needed to prevent undercounting due to simultaneous muon arrivals. The time width of a light signal produced by a muon (for AMIGA MCs less than 25 ns to 35 ns [14]), is defined by the convolution of the probability distributions characterized by the decay time of the scintillator, the decay time of the optical fiber, and to lesser extend the propagation mode in the optical fiber.

A SiPM model and a new electronics for the readout of AMIGA MCs are proposed in the next two sections, based on these specifications and the experience of the current version of the AMIGA electronics [15, 16].

3.1 SiPM Selection

Two main features which improve the signal-to-noise ratio were taken into account in order to select the specific device: high photo-detection efficiency (PDE) and low noise. The PDE of the selected devices is around 35 % for the emission wavelength of the fiber optic (485 nm). Low noise is obtained by combining low dark rate with reduced cross-talk and low afterpulsing probability.

Three devices manufactured by Hamamatsu (S12572-100C, S12571-100C, S13081-050CS) were tested in the laboratory to evaluate their performance. In Figure 2 an overlap of 5000 dark rate traces of each SiPM model is shown. Pulses of more than one SPE, stacked due to cross-talk, can be observed synchronized with the trigger time. Afterpulsing pulses can also be observed after the trigger time.

The three SiPMs exemplified are some of the latest devices developed by Hamamatsu up to 2015. The second SiPM (S12571-100C) in figure 2 shows a reduction in the afterpulsing probability compared to the first one (S12572-100C). The third model (S13081-050CS) not only shows a reduction in the afterpulsing, but also a significantly lower value of cross-talk. The main characteristics of these SiPMs, obtained from the Hamamtsu datasheets, are summarized in table 3.1.

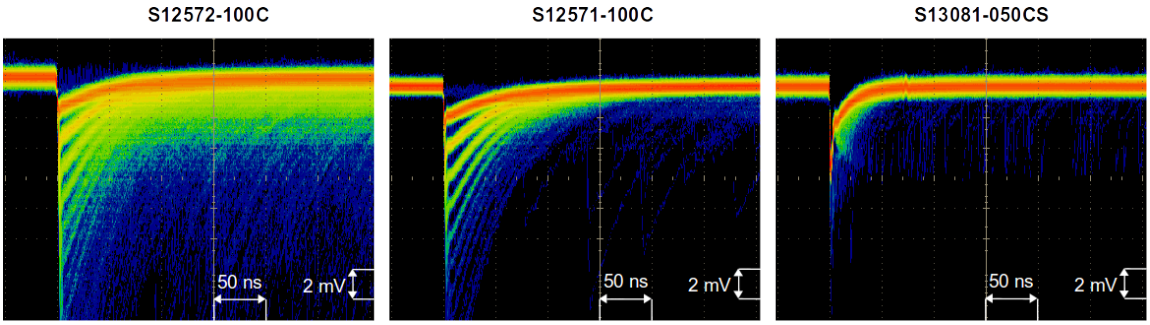

Figure 2. Overlap of 5000 dark rate traces (signal amplitude as a function of time) of each SiPM model. All measurements were done with the same amplifier at 25 °C. The ΔV of each SiPM was set to the value recommended by Hamamatsu.

The criteria selected for counting muons is to count pulses above a given threshold. In this context, cross-talk probability becomes a relevant parameter. This correlated noise makes possible that a pulse triggered by dark noise or afterpulsing could have an amplitude above the selected threshold. Therefore, cross-talk should be as small as possible to reduce the accidental counting probability. The selected device for this work was the third model (S13081-050CS) mainly due to its low cross-talk probability and also its low dark noise and afterpulsing.

Parameter		**SiPM Model**			**Unit**
		S12572-100C	S12571-100C	S13081-050CS	
Cell Pitch		100	100	50	μm
Effective Photosensitive Area		3 x 3	1 x 1	1.3 x 1.3	mm
Geometrical Fill Factor		78.5	78	61	%
Photon Detection Efficiency		35	35	35	%
Number of Cells		900	100	667	-
Dark Count	Typ.	1000	100	90	kcps
	Max.	2000	200	360	kcps
Gain M		2.8×10^6	2.8×10^6	1.5×10^6	-
Gain Temperature Coefficient		1.2×10^5	1.2×10^5	2.7×10^4	$/°C$
Breakdown Voltage		65 ± 10	65 ± 10	53 ± 5	V
Cross-Talk Probability		35	35	1	%

Table 3.1. Main characteristics, obtained from the Hamamatsu datasheets, of the three tested SiPMs: S12571-100C [17], S12572-100C [18] and S13081-050CS [19].

3.2 Proposed Electronics

The proposed electronics is based on the existing AMIGA system. The following main specifications were considered for the design:

1. Control over the threshold discriminators of each channel.
2. Independent bias voltage control for each channel.

3. Non-inverting (positive polarity signals).

4. Low power consumption (stand-alone power system).

5. A fast shaper trigger with a maximum width of ~25 ns - 35 ns (digital output) for the maximum muon signal. The fast shaper trigger must be able to discern three or more SPEs in a ~25 ns - 35 ns window mounted on the remnants of any decaying previous muon signal.

6. Temperature compensation (SiPM breakdown voltage depends on temperature).

The *Application Specific Integrated Circuit* (ASIC) *Cherenkov Imaging Telescope Integrated Read Out Chip* (CITIROC) [20] was proposed for the front-end readout of AMIGA because it was specifically designed for the readout of SiPMs and also fulfils the requirements needed for AMIGA detectors. For the biasing and temperature compensation of each SiPM, the Hamamatsu C11204-01 power supply [21] was selected due to the recommendation of Hamamatsu.

The CITIROC is a 32 channel front-end and it has an 8-bit input digital-to-analog converter (DAC) which can be used to modify each SiPM bias voltage. Each channel has a pre-amplifier stage that can be selected by software between a low or high gain pre-amplifier. Also each corresponding gain value is programmable. Then the signal passes through a 15 ns peaking time fast shaper followed by a discriminator. The discriminator threshold is set coarsely by a 10-bit DAC (common for the 32 channels) and then set finely channel by channel by individual 4-bit DACs.

4 Calibration Method of the Counting System

The calibration method of the counting system for AMIGA is split into two steps. The first step consists in calibrating the optical sensors of each individual channel (see subsection 4.1) and the second step consists in calibrating the detector (see subsection 4.2).

4.1 SiPM Calibration

This is the first step of the calibration needed in the counting system. The goal is to set the operation point of the SiPMs. First, the breakdown voltage of each individual channel must be obtained. Then, all the SiPMs must be biased to its corresponding breakdown voltage with an added predetermined overvoltage. This overvoltage can be changed to optimize the efficiency. In this section a method for obtaining the breakdown voltage and biasing of the SiPMs with the proposed AMIGA electronics is explained.

4.1.1 SiPM Calibration Setup

The setup for the SiPMs calibration is divided into three stages (see figure 3). The first stage is composed of the SiPM, the high voltage power supply and the temperature sensor. Since the SiPM breakdown voltage varies significantly with temperature, the high voltage power supply has a built-in high precision temperature compensation system that constantly corrects the SiPM operation point. This function tries to keep the gain value fixed independently of temperature variations. The compensation of the high voltage (HV) output is determined by the equation 4.1 (given by Hamamatsu). In this formula, the $\Delta T'$ and ΔT are respectively the quadratic and linear coefficients

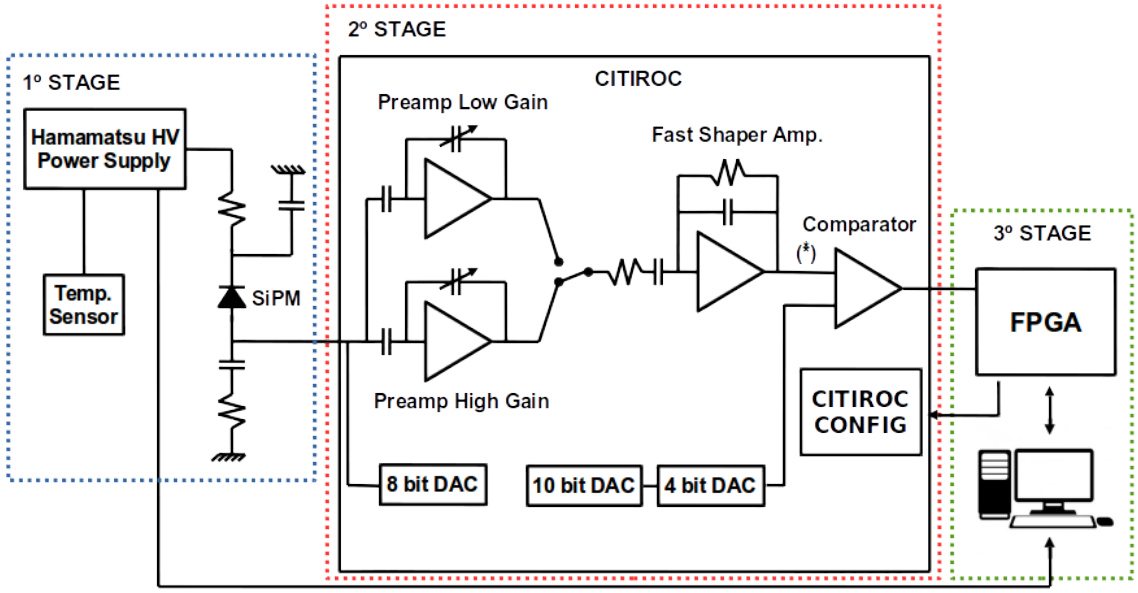

Figure 3. SiPM Calibration Setup. The three stages are distinguished with dotted lines. The output of the fast shaper amplifier (∗) has a DC offset component.

for the temperature compensation, and V_b is the reference voltage. For the SiPMs under test $\Delta T'$ was set to $0\,\mathrm{mV/^\circ C^2}$, ΔT to $54\,\mathrm{mV/^\circ C}$ and the reference temperature (T_b) to $25\,^\circ\mathrm{C}$. The resulting formula for the calibration is described in equation 4.2.

The second stage consists of the CITIROC. This stage amplifies and then discriminates SiPM pulses. The chip was programmed to use the high gain pre-amplifier, with its maximum gain of 10, to improve the separation between SPEs in the SPE spectrum. The 8-bit DAC input was set to a fixed value (e.g. 250 dac-units). The 10-bit DAC was used to set the comparator threshold for all the channels and the 4-bit DAC of each channel was fixed to its minimum value.

$$HV = \Delta T' * (T - T_b)^2 + \Delta T * (T - T_b) + V_b \tag{4.1}$$

$$HV = 54\,mV/^\circ C * (T - 25\,^\circ C) + V_b \tag{4.2}$$

The third stage is composed of a FPGA. The FPGA was programmed to measure the rate of the CITIROC digital pulses output.

4.1.2 Single Photon Equivalent Peak Measurement

To be able to perform the calibration proposed in this subsection, a difference in the rate value of one SPE and two SPEs is needed. A dedicated software was developed to automatically measure the rate of the digital pulses at different discrimination levels. In the measurement of the SiPM noise rate as a function of the 10-bit DAC values (see figure 4, left) there is a clear transition from the first to the second plateau. This transition represents the threshold of the comparator passing through the first SPE peak.

The absolute value of the derivative of this curve (see figure 4, right) represents the distribution of the SPE peak values. The mean value of the SPE peak (D_{max}) is correlated to the maximum

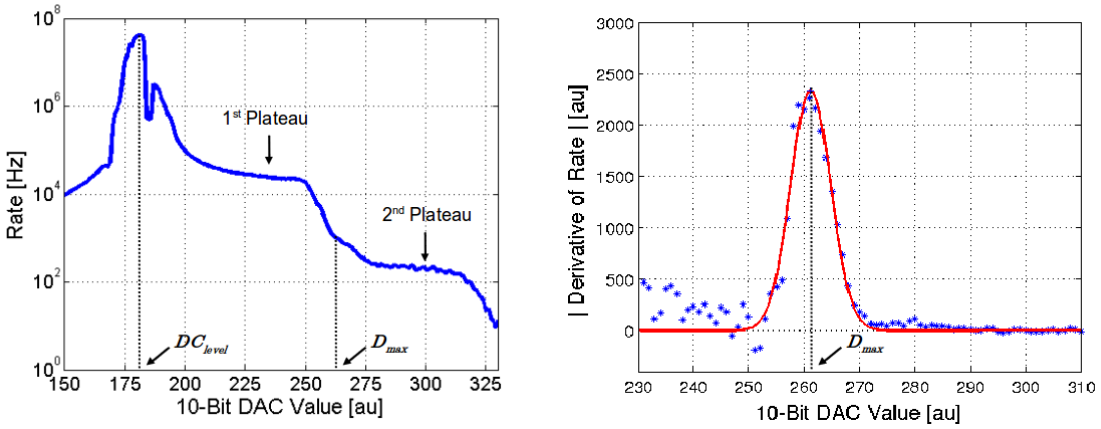

Figure 4. On the left, the measurement of the rate of the SiPM pulses as a function of the DAC value. DC_{level} corresponds to the fast shaper DC offset component. See subsection 4.1.1 for details on the setup. On the right, the absolute value of the derivative of the rate evidences the mean value of the peak (D_{max}), obtained with a Gaussian fit of the points (red curve).

absolute value of the Gaussian distribution coming from the derivative of the rate curve. This value has an offset (DC_{level}) because the signal in the fast shaper has a DC offset component (see figure 3). The value of this DC offset is the DAC value where the rate is maximum (see figure 4, left). To obtain the real value of the SPE peak it is necessary to subtract this offset (see equation 4.3).

$$SPE_{peak} = D_{max} - DC_{level} \tag{4.3}$$

As was mentioned before, the employment of SiPMs combined with the method explained in this subsection, allow the SPE_{peak} estimation which is used to calculate the breakdown voltage of the device, as will be explained in the next subsection.

4.1.3 Breakdown Voltage Measurements

There are several methods to estimate the breakdown voltage of a SiPM [22]. Due to the constrain of the proposed electronics, the method to estimate each channel breakdown voltage is the one described in this subsection.

Equations 2.1 and 2.2 are summarized in figure 5, left. This figure shows that if the gain (M) is measured over the V_{bias}, the breakdown voltage can be obtained as the value where the curve intercepts the X axis ($V_{bias} = V_{BR}$). It is also known that the SPE_{peak} is directly proportional to the gain (Mean $SPE_{peak} \propto$ M). By using this information and following the procedure explained in the previous subsection, a plot of SPE_{peak} for different V_{bias} values, can be obtained. An example for four different SiPMs is shown in figure 5, right. From that plot, the V_{BR} can be estimated as the point where the linear fit of the curve intercepts the X axis ($HV\ set \equiv V_{bias} = V_{BR}$).

To automatize the breakdown voltage estimation, the 8-bit DAC input of the CITIROC (see figure 3) was fixed to 250 dac-units for all the channels and the HV value was changed (V_{bias} changes following the power supply HV). With this method, it is possible to calculate each SiPM characteristic breakdown voltage at the same time, with a single power supply. This is the case

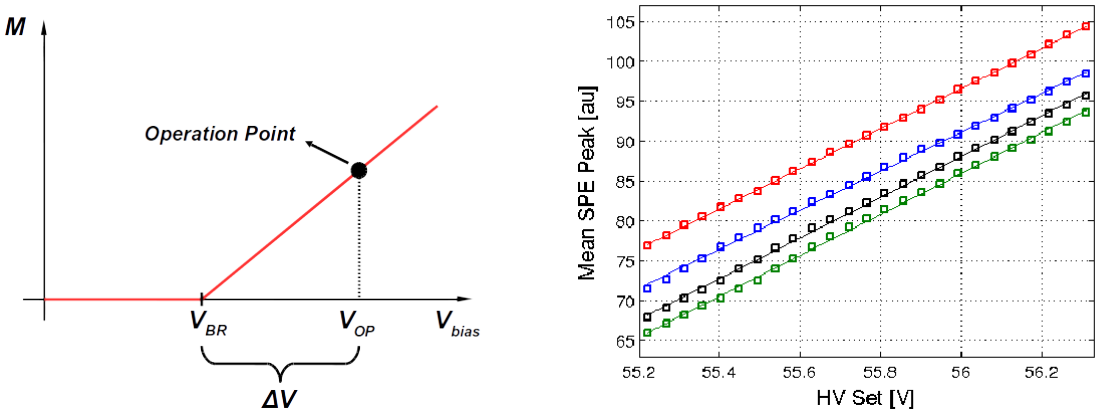

Figure 5. The plot on the left summarizes equations 2.1 and 2.2. The mean SPE_{peak} as a function of the HV value for four different SiPMs is plotted on the right. The mean SPE_{peak} is proportional to M, and HV Set represents the V_{bias}.

with the electronics that will be deployed. In the following subsection a possible equalization of SiPMs overvoltage is explained following this constraint.

4.1.4 Equalization Between Channels

As was mentioned before, the ΔV applied to each device is the only parameter that can be changed to modify the characteristics of the SiPM behaviour, for a fixed temperature. Therefore, it is desirable for all the SiPMs in the detector to have the same ΔV applied. The equalization consists in applying the same ΔV to all the channels. This equalization does not ensure the same gain or rate at a given threshold between channels.

Since the designed electronics has only one power supply and considering that the SiPMs have different V_{BR}, in order to set the desired operation voltage (V_{OP}) for each SiPM individually, the following procedure is carried out:

1. Set the HV voltage of the power supply to the largest V_{BR} of the 64 SiPMs with the desired ΔV added (see equation 4.4).

2. Change the voltage setting individually by the 8-bit DAC input of the CITIROC ($V_{8bitDAC}$) for each SiPM (represented by index i). Combining equations 4.4 and 4.5, equation 4.6 can be obtained. In this last equation, the $V_{8bitDAC}$ value that must be set is shown.

$$HV = V_{BR_{max}} + \Delta V \tag{4.4}$$

$$HV - V_{8bitDAC_i} = V_{BR_i} + \Delta V = V_{OP_i} \tag{4.5}$$

$$V_{8bitDAC_i} = V_{BR_{max}} - V_{BR_i} \tag{4.6}$$

4.2 Detector Calibration

Once the SiPM is calibrated, the next step consists of determining the discrimination level and the counting strategy (detector calibration), ensuring an adequate performance of the counting system.

4.2.1 Detector Calibration Setup

The setup for the detector calibration is divided into six stages (see figure 6). The first stage is the same as the first stage described in the subsection 4.1.1. The second stage is composed of the stages two and three described in the subsection 4.1.1. For this calibration, the CITIROC was programmed to use the high gain pre-amplifier, with its minimum gain of one, to reduce the digital time span of the discriminated pulses. The 4-bit DAC was fixed to its minimum value and the 8-bit DAC input was set following the procedure detailed in the subsection 4.1.4 (equalization). The 10-bit DAC is used to set different discrimination levels. The third stage is an amplifier to allow the measurement of the analog signal of the SiPM. The fourth stage consists of a 4 m plastic scintillation bar with a 5 m wavelength-shifting optical fiber threaded, as the ones the muon counter is built of. At the end of the optical fiber there is an optical connector coupled to the SiPM. The fifth stage is a muon telescope trigger [23] that ensures the acquisition occurs every time a particle passes through each position of the scintillator where the telescope is placed. The sixth stage is the acquisition system. This stage is composed of a Tektronix DPO7104 oscilloscope. This oscilloscope is set up to store the discriminated signal of the CITIROC (stage 2) and the amplified analog signal of the SiPM (stage 3) every time the muon telescope produces a coincidence in a time window of 60 ns (stage 5).

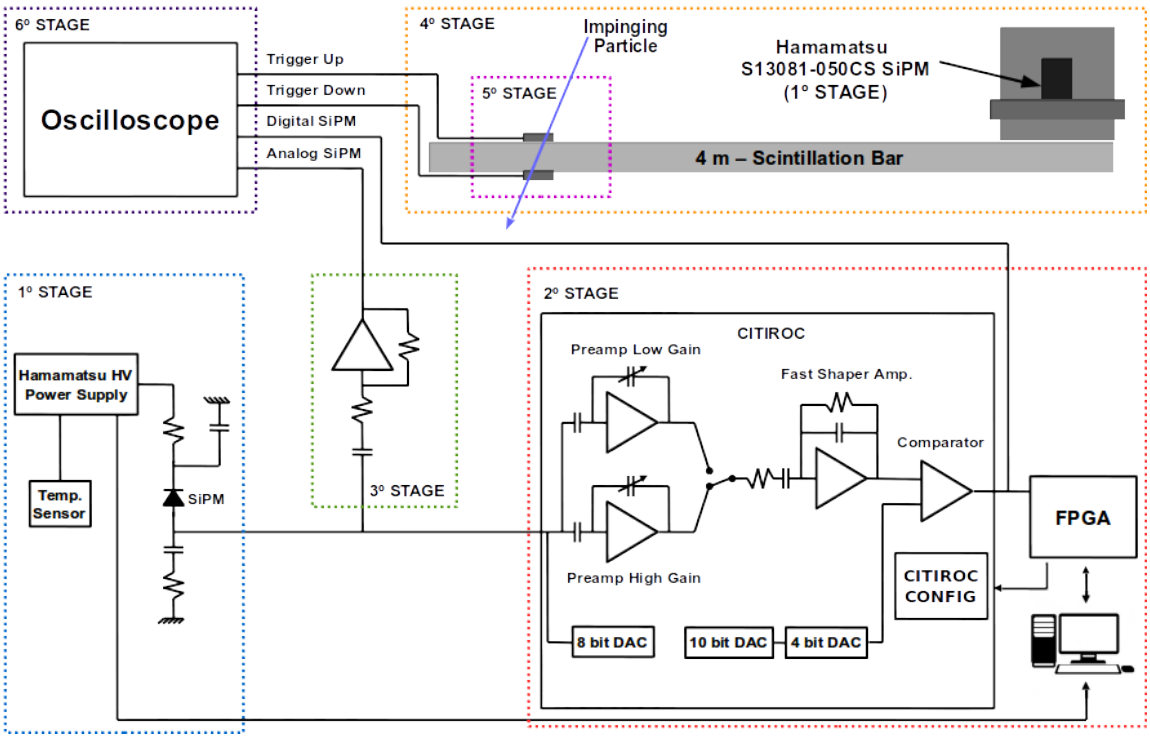

Figure 6. The six stages of the setup needed for the detector calibration. The 4 m plastic scintillation bar has a 5 m wavelength-shifting optical fiber threaded. The difference in length is due to the extra fiber needed to reach the optical connector.

4.2.2 Selection of the Counting Strategy

As was described in [24] the current counting system (PMT and electronics) is conceived to count muons by identifying a pattern in the digital trace. The discrimination level is set at a value lower than one SPE and then a pattern recognition technique is applied to discriminate particles from noise. This counting strategy takes into account the time structure of the signal over a threshold.

The proposed counting strategy for the SiPMs is based on an amplitude criteria. The high PDE (~35 %) of these devices at the emission wavelength of the WLS optical fiber allows setting a threshold of a small number of SPEs to discriminate particles from noise, without losing particle detection efficiency.

The discrimination level is set at the lowest value that ensures a low rate of contamination (negligible accidental counting) and also does not damage the counting efficiency. In figure 7, the rate of SiPM pulses as a function of the 10-bit DAC threshold is shown. Two cases are plotted: in red the rate when the fiber is coupled to the SiPM, and in blue when it is not. When the fiber is not coupled to the SiPM, only the noise from the SiPM is measured. When the fiber is coupled to the SiPM, not only the dark rate and its correlated noise is measured, but also all the signals produced by charged particles impinging the scintillator. These particles will be considered as the environmental radiation. In figure 7, for one and two SPE rate levels, the correlated and the uncorrelated noises, explained in section 2.1, dominate. If the threshold level is set in any of these values, the accidental counting probability for the whole detector (64 channels) is over the desired limit level of 5 %. At three SPE rate level, the environmental radiation starts to dominate over the noise. For this level, the accidental counting probability (see equation 4.8) is mainly due to the environmental radiation and fulfils the requirement, therefore this is the selected level for the threshold.

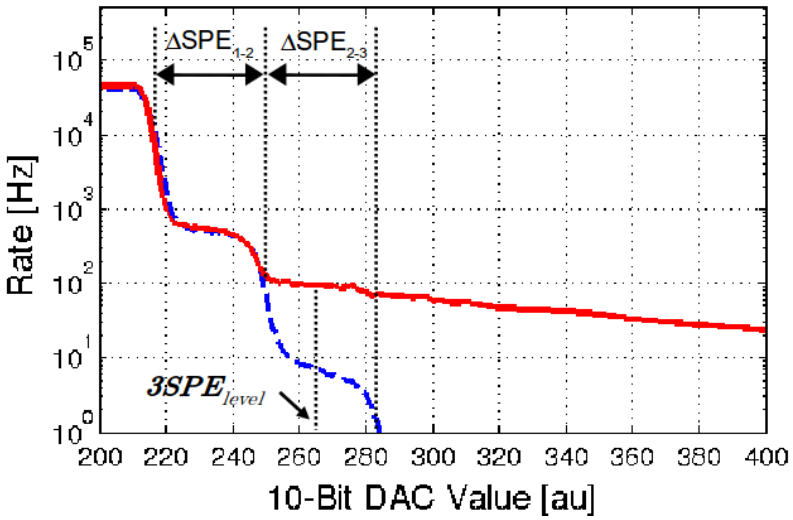

Figure 7. Measurement of the SiPM pulses rate with (red complete line) and without (blue dashed line) the scintillating bar over the 10-bit DAC value. Each plateau represents the transition for different amounts of SPEs. The value marked with the $3SPE_{level}$ is the selected value for the threshold of the discriminator.

As it was mentioned in subsection 4.1.2, the transition between plateaus in the SiPM rate as

a function of the 10-bit DAC value represents the threshold of the comparator passing through the SPE peaks. Furthermore, as was mentioned in section 2, the amplitude of the signal generated by multiple simultaneously fired cells is directly proportional to the number of them. Therefore, it is expected that: $\Delta SPE_{1-2} = \Delta SPE_{2-3} = SPE_{peak}$ (see figure 7). In the example shown, the obtained values were: $\Delta SPE_{1-2} = (32 \pm 2)$; $\Delta SPE_{2-3} = (36 \pm 2)$; $SPE_{peak} = (34 \pm 2)$ (in arbitrary units). Taking into account the uncertainties in the measurement, they are all compatible.

The middle point of the transition from the second to the third SPE peaks ($SPE_{peak} * 2.5$) corresponds to the value that ensures the detection of signals with three or more SPEs ($3SPE_{level}$). Considering the offset (DC_{level}), this value can be calculated with equation 4.7.

$$3SPE_{level} = SPE_{peak} * 2.5 + DC_{level} \simeq (34 \pm 2) * 2.5 + (182 \pm 1) = 267 \pm 6 \tag{4.7}$$

As an example, in the case exemplified in figure 7 the estimated SPE_{peak} was (34 ± 2) and the DC_{level} was (182 ± 1). The calculated $3SPE_{level}$ value is indicated in the figure, and it corresponds to the middle point of the third SPE plateau. The $3SPE_{level}$ must be estimated and set individually for each channel.

$$P_{accidental-counting} = n \cdot T_{event} \cdot R_{noise} \simeq 64 \cdot 3.2\,\mu s \cdot 100\,Hz \equiv 2.05\,\% \tag{4.8}$$

To estimate the accidental counting probability ($P_{accidental-counting}$) three factors are taken into account: the segmentation (n), the acquired event time window (T_{event}) and the noise rate (R_{noise}, i.e. the environmental radiation and dark rate). As an example, for the AMIGA modules the segmentation is of 64 channels, the acquired event time window is 3.2 μs and the noise rate in the laboratory is ~100 Hz (this value is the rate corresponding to $3SPE_{level}$ in figure 7). With those values the accidental counting probability for a 10 m^2 module was estimated to be ~2 % (see equation 4.8). The efficiency will be studied in detail in section 5.

4.3 Proposed On-site Calibration

The electronics design enables calibration to be performed at the observatory site. To ensure their long-term performance, both calibrations detailed in sections 4.1 and 4.2 will be applied regularly and automatically. Each module will acquire the data locally and then send it to a dedicated calibration server that will be running in the Central Data Acquisition System (CDAS) of the Pierre Auger Observatory. This calibration server will carry out the SiPM calibration as well as the detector calibration. This dedicated server will do the calculations to set three groups of parameters: the HV value, the 8-bit DAC input to equalize the channels, and the 10-bit DAC value to set the discrimination level. All the calibration data and the parameters obtained will be stored for long-term stability studies.

5 Efficiency Measurements

As mentioned in section 1, the module must count efficiently the number of impinging muons. To test its efficiency, the setup described in subsection 4.2.1 was used. Several measurements at different fiber lengths were taken using the muon telescope.

The efficiency is defined as the ratio between the digital output of the CITIROC, and the number of triggers of the muon telescope, that ensures a particle passing through the scintillation bar at a certain distance. At the same time, the amplified analog pulses were stored as well.

A histogram illustrating the amplitude peak and charge of the traces obtained at a fiber distance of 406 cm with the S13081-050CS SiPM is shown in figure 8. Both plots were obtained from the analog signal of the SiPM. Three coloured areas can be distinguished in each histogram. The red area corresponds to the analog traces that do not have a corresponding digital output of the CITIROC. This means that no particle was detected by the counting system. The green area are all the pulses that have a digital output. The blue area is the sum of the red and green areas. Due to the discrimination applied by the electronics, the traces that have a charge and peak lower than the threshold level did not produce a digital output on the CITIROC.

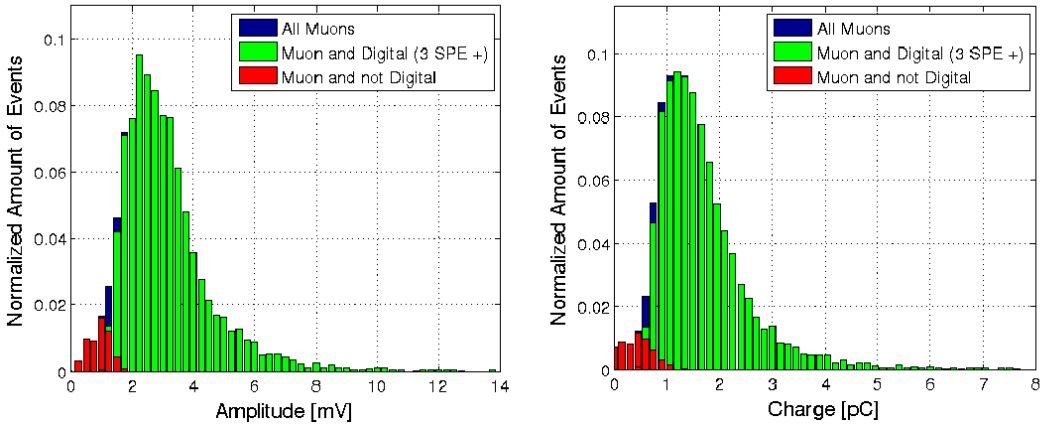

Figure 8. In the left (right) plot, the amplitude (charge) histogram of 1000 analog traces is shown. The red coloured area corresponds to the analog traces that do not have a digital output. All the measurements were done at 25 °C, $\Delta V = 3.75\,V$, and with the muon telescope placed at 406 cm of fiber from the SiPM.

Both plots in figure 9 show the linear correlation between amplitude and charge of SiPM signals. This is a strong evidence of the superposition of the individual photons produced by the particle passing through the detector. In these plots there is also a discrimination between the traces with (blue) or without (red) digital output. In the left plot, the results with the muon telescope placed at 406 cm of fiber are shown, and in the right one, the muon telescope was moved to 106 cm. As expected, the data sets have higher mean amplitude and charge values due to a decrease in the attenuation of light in the fiber.

In figure 10, the time width of the digital output traces at both fiber distances measured is shown. As it was pointed out in the requirements, 98 % of the digital widths are lower than 35 ns. This requirement was achieved by the fast shaper included in the CITIROC.

There are two main factors that constrain the performance of the detector. Since the light yield is not uniform, both limits of the scintillation bar have different characteristics. In the farther distances the efficiency strongly depends on the threshold selection, since the attenuation of the optical fiber significantly decreases the number of photons that arrive to the SiPM. At the closest distances the number of detected photons is higher and the digital width is consequently increased.

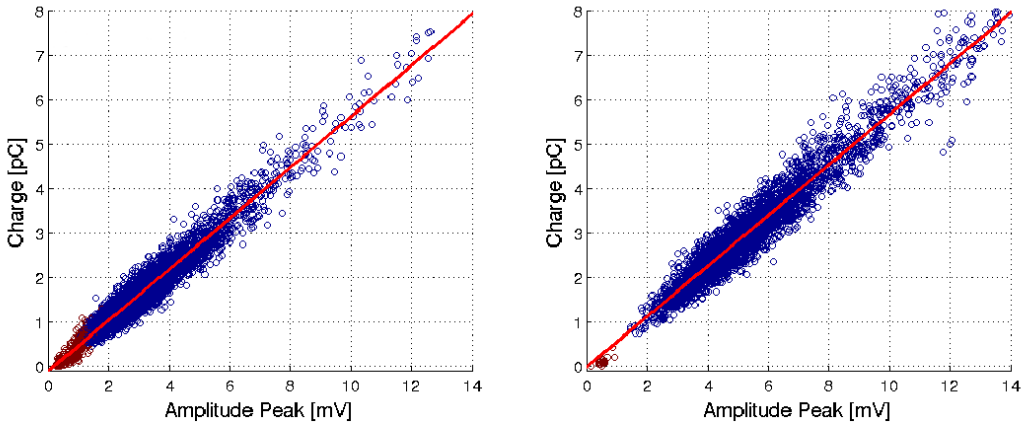

Figure 9. Both plots show the relationship between the amplitude and the charge of 1000 analog traces. The red coloured points correspond to the analog traces that do not have a digital output. In the left (right) plot the muon telescope was placed at 406 cm (106 cm) of fiber. All the measurements were done at 25 °C and $\Delta V = 3.75\,V$.

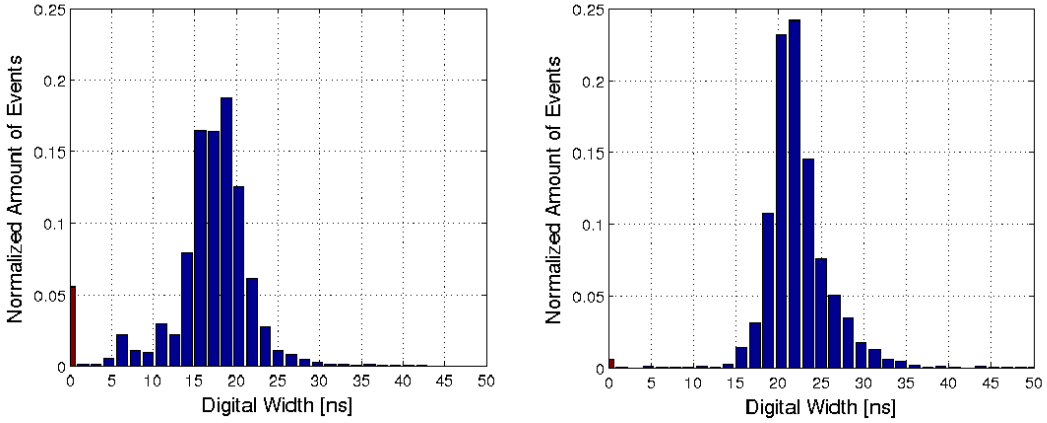

Figure 10. Both plots show the digital output width histogram of 1000 digital traces. The red coloured bar corresponds to the traces that do not have a digital output pulse. In the left (right) plot the muon telescope was placed at 406 cm (106 cm) of fiber. All the measurements were done at 25 °C and $\Delta V = 3.75\,V$.

The selected pre-amplifier gain combined with the fast shaper ensures an adequate width of the digital output.

5.1 Efficiency Results and Possible Improvements

As described in the previous subsection, the efficiency of the particle detection was evaluated at different fiber lengths. Figure 11 summarizes the results for five different distances.

To improve the efficiency, a higher ΔV was tested, since the PDE of the SiPM rises with the increment of the ΔV. With the increment of the ΔV, the noise is also increased. The ΔV was chosen ensuring that the accidental counting value remains below the 5 % requirement and the efficiency is as high as possible.

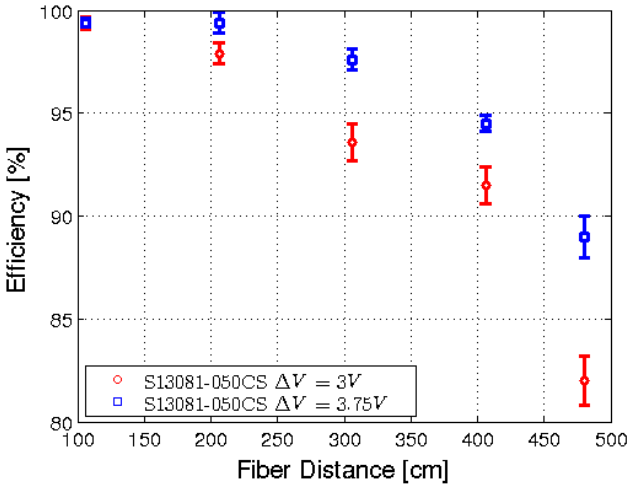

Figure 11. Efficiency measurements for two different ΔV are compared. A larger ΔV produces an increase in the efficiency. The estimated integrated efficiency is: 93 % for $\Delta V = 3\,V$ (red) and 96 % for $\Delta V = 3.75\,V$ (blue).

Despite the individual values at different distances, the main parameter that should be calculated is the integrated efficiency over the whole scintillation bar. For the two cases exemplified in figure 11, the estimated integrated efficiency was: 93 % for $\Delta V = 3\,V$ and 96 % for $\Delta V = 3.75\,V$.

6 Conclusions

A new readout for the AMIGA muon counters was proposed fulfilling the requirements imposed by the AMIGA detector design. The selected SiPM was the S13081-050CS due to its low crosstalk and afterpulsing. The CITIROC ASIC was selected as the electronics front-end and the Hamamatsu C11204-01 power supply was chosen for the biasing of the SiPMs.

The proposed calibration method consist of two steps. Firstly, the SiPM calibration allows the individual characterization of each SiPM of the module and the equalization between channels. Secondly, the detector calibration determines the discrimination level and the counting strategy. Both calibrations combined guarantee the performance of the detector by an adequate overvoltage and threshold level selection. Both methods were designed to be performed on the Observatory site. This allows studying the long-term performance of the detector, improving its stability for long periods.

Laboratory efficiency studies show promising results. The high integrated efficiency obtained (96 % for the higher tested overvoltage) combined with a low probability of accidental counting (~2 %) evidences an adequate performance of the proposed counting system.

Acknowledgments

The successful installation, commissioning, and operation of the Pierre Auger Observatory would not have been possible without the strong commitment and effort from the technical and admin-

istrative staff in Malargüe. We are very grateful to the following agencies and organizations for financial support:

Comisión Nacional de Energía Atómica, Agencia Nacional de Promoción Científica y Tecnológica (ANPCyT), Consejo Nacional de Investigaciones Científicas y Técnicas (CONICET), Gobierno de la Provincia de Mendoza, Municipalidad de Malargüe, NDM Holdings and Valle Las Leñas, in gratitude for their continuing cooperation over land access, Argentina; the Australian Research Council; Conselho Nacional de Desenvolvimento Científico e Tecnológico (CNPq), Financiadora de Estudos e Projetos (FINEP), Fundação de Amparo à Pesquisa do Estado de Rio de Janeiro (FAPERJ), São Paulo Research Foundation (FAPESP) Grants No. 2010/07359-6 and No. 1999/05404-3, Ministério de Ciência e Tecnologia (MCT), Brazil; Grant No. MSMT CR LG15014, LO1305 and LM2015038 and the Czech Science Foundation Grant No. 14-17501S, Czech Republic; Centre de Calcul IN2P3/CNRS, Centre National de la Recherche Scientifique (CNRS), Conseil Régional Ile-de-France, Département Physique Nucléaire et Corpusculaire (PNC-IN2P3/CNRS), Département Sciences de l'Univers (SDU-INSU/CNRS), Institut Lagrange de Paris (ILP) Grant No. LABEX ANR-10-LABX-63, within the Investissements d'Avenir Programme Grant No. ANR-11-IDEX-0004-02, France; Bundesministerium für Bildung und Forschung (BMBF), Deutsche Forschungsgemeinschaft (DFG), Finanzministerium Baden-Württemberg, Helmholtz Alliance for Astroparticle Physics (HAP), Helmholtz-Gemeinschaft Deutscher Forschungszentren (HGF), Ministerium für Wissenschaft und Forschung, Nordrhein Westfalen, Ministerium für Wissenschaft, Forschung und Kunst, Baden-Württemberg, Germany; Istituto Nazionale di Fisica Nucleare (INFN),Istituto Nazionale di Astrofisica (INAF), Ministero dell'Istruzione, dell'Universitá e della Ricerca (MIUR), Gran Sasso Center for Astroparticle Physics (CFA), CETEMPS Center of Excellence, Ministero degli Affari Esteri (MAE), Italy; Consejo Nacional de Ciencia y Tecnología (CONACYT) No. 167733, Mexico; Universidad Nacional Autónoma de México (UNAM), PAPIIT DGAPA-UNAM, Mexico; Ministerie van Onderwijs, Cultuur en Wetenschap, Nederlandse Organisatie voor Wetenschappelijk Onderzoek (NWO), Stichting voor Fundamenteel Onderzoek der Materie (FOM), Netherlands; National Centre for Research and Development, Grants No. ERA-NET-ASPERA/01/11 and No. ERA-NET-ASPERA/02/11, National Science Centre, Grants No. 2013/08/M/ST9/00322, No. 2013/08/M/ST9/00728 and No. HARMONIA 5 – 2013/10/M/ST9/00062, Poland; Portuguese national funds and FEDER funds within Programa Operacional Factores de Competitividade through Fundação para a Ciência e a Tecnologia (COMPETE), Portugal; Romanian Authority for Scientific Research ANCS, CNDI-UEFISCDI partnership projects Grants No. 20/2012 and No.194/2012 and PN 16 42 01 02; Slovenian Research Agency, Slovenia; Comunidad de Madrid, Fondo Europeo de Desarrollo Regional (FEDER) funds, Ministerio de Economía y Competitividad, Xunta de Galicia, European Community 7th Framework Program, Grant No. FP7-PEOPLE-2012-IEF-328826, Spain; Science and Technology Facilities Council, United Kingdom; Department of Energy, Contracts No. DE-AC02-07CH11359, No. DE-FR02-04ER41300, No. DE-FG02-99ER41107 and No. DE-SC0011689, National Science Foundation, Grant No. 0450696, The Grainger Foundation, USA; NAFOSTED, Vietnam; Marie Curie-IRSES/EPLANET, European Particle Physics Latin American Network, European Union 7th Framework Program, Grant No. PIRSES-2009-GA-246806; and UNESCO.

References

[1] The Pierre Auger Collaboration, *The Pierre Auger Cosmic Ray Observatory*, *NIM A* **798** (2015) 172-213 [doi:10.1016/j.nima.2015.06.058].

[2] I. Allekotte, A. F. Barbosa, P. Bauleo, C. Bonifazi, B. Civit, C. O. Escobar, B. García, G. Guedes, M. Gómez-Berisso, J. L. Harton, M. Healy, M. Kaducak, P. Mantsch, P. O. Mazur, C. Newman-Holmes, I. Pepe, I. Rodriguez-Cabo, H. Salazar, N. Smetniansky-De Grande, D. Warner, for the Pierre Auger Collaboration, *The Surface Detector System of the Pierre Auger Observatory*, *NIM A* **586** (2008) 409-420 [doi:10.1016/j.nima.2007.12.016].

[3] The Pierre Auger Collaboration, *The Fluorescence Detector of the Pierre Auger Observatory*, *NIM A* **620** (2010) 227-251 [doi:10.1016/j.nima.2010.04.023].

[4] A. Etchegoyen for the Pierre Auger Collaboration, *AMIGA, Auger Muons and Infill for the Ground Array*, *Published as Proceedings of 30th ICRC*, Mérida, México, **5** (2007) 1191-1194 [arXiv:0710.1646].

[5] M. Platino for the Pierre Auger Collaboration, *AMIGA, Auger Muons and Infill for the Ground Array of the Pierre Auger Observatory*, *Published as Proceedings of 31st ICRC*, Łódź, Poland, **5** (2009) 14-17 [arXiv:0906.2354].

[6] P. Buchholz for the Pierre Auger Collaboration, *Hardware Developments for the AMIGA enhancement at the Pierre Auger Observatory*, *Published as Proceedings of 31st ICRC*, Łódź, Poland, **5** (2009) 22-25 [arXiv:0906.2354].

[7] The KASCADE Collaboration, *The cosmic-ray experiment KASCADE*, *NIM A* **513** (2003) 490-510 [doi:10.1016/S0168-9002(03)02076-X].

[8] The KASCADE-Grande Collaboration, *The KASCADE-Grande experiment*, *NIM A* **620** (2010) 202-216 [doi:10.1016/j.nima.2010.03.147].

[9] The Pierre Auger Collaboration, *Prototype muon detectors for the AMIGA component of the Pierre Auger Observatory*, *JINST* **11** (2016) P02012 [doi:10.1088/1748-0221/11/02/P02012].

[10] S. Piatek, Hamamatsu Corporation & New Jersey Institute of Technology, *Physics and Operation of an MPPC*, (2014).

[11] P. Eckert et al., *Characterisation Studies of Silicon Photomultipliers*, *NIM A* **620** (2010) 217-226 [doi:10.1016/j.nima.2010.03.169]

[12] S. M. Sze and K. K. Ng, *Physics of Semiconductor Devices*, *NJ: Wiley-Interscience* (2007) [ISBN:978-0-471-14323-9]

[13] A. D. Supanitsky, A. Etchegoyen, G. Medina-Tanco, I. Allekotte, M. Gómez Berisso, M. C. Medina, *Underground Muon Counters as a Tool for Composition Analyses*, *Astroparticle Physics* **29** (2008) 461-470 [doi:10.1016/j.astropartphys.2008.05.003].

[14] B. Wundheiler for the Pierre Auger Collaboration, *The AMIGA muon counters of the Pierre Auger Observatory: performance and first data*, *Published as Proceedings of 32nd ICRC*, Beijing, China, (2011) #0341 [doi:10.1088/1742-6596/375/1/052006].

[15] O. Wainberg et al., *Digital electronics for the Pierre Auger Observatory AMIGA muon counters*, *JINST* **9** (2014) T04003 [doi:10.1088/1748-0221/9/04/T04003].

[16] A. Almela et al., *Design and implementation of an embedded system for particle detectors*, *Published as Proceedings of 33rd ICRC*, Rio de Janeiro, Brazil, (2013) #1209 [ISBN:978-85-89064-29-3].

[17] Hamamatsu Photonics K.K., *MPPC Multi-pixel photon counter, S12571-25, -50, -100C/P specification datasheet*, (2015).

[18] Hamamatsu Photonics K.K., *MPPC Multi-pixel photon counter, S12572-25, -50, -100C/P specification datasheet*, (2015).

[19] Hamamatsu Photonics K.K., *MPPC Multi-pixel photon counter, S13081-050CS, S13081-050PE specification datasheet*, (2015).

[20] Omega Micro CNRS-IN2P3-Ecole Polytechnique, *CITIROC Front-end Chip*, (2014).

[21] Hamamatsu Photonics K.K., *Power supply for MPPC*, (2015).

[22] V. Chmill et al., *Study of the breakdown voltage of SiPMs*, *Instrumentation and Detectors (physics.ins-det)* (2016) 047 [doi:10.1016/j.nima.2016.04.047]

[23] M. Platino et al., *AMIGA at the Auger Observatory: the scintillator module testing system*, *JINST* (2011) P06006 [doi:10.1088/1748-0221/6/06/P06006]

[24] B. Wundheiler for the Pierre Auger Collaboration, *The AMIGA muon counters of the Pierre Auger Observatory: Performance and Studies of the Lateral Distribution Function*, *Published as Proceedings of 34th ICRC*, The Hague, The Netherlands, (2015) #0324 [arXiv:1509.03732].

The Pierre Auger Collaboration

A. Aab[37], P. Abreu[70], M. Aglietta[48,47], E.J. Ahn[85], I. Al Samarai[29], I.F.M. Albuquerque[16], I. Allekotte[1], P. Allison[90], A. Almela[8,11], J. Alvarez Castillo[62], J. Alvarez-Muñiz[80], M. Ambrosio[45], G.A. Anastasi[38], L. Anchordoqui[84], B. Andrada[8], S. Andringa[70], C. Aramo[45], F. Arqueros[77], N. Arsene[73], H. Asorey[1,24], P. Assis[70], J. Aublin[29], G. Avila[9,10], A.M. Badescu[74], A. Balaceanu[71], C. Baus[32], J.J. Beatty[90], K.H. Becker[31], J.A. Bellido[12], C. Berat[30], M.E. Bertaina[56,47], X. Bertou[1], P.L. Biermann[b], P. Billoir[29], J. Biteau[28], S.G. Blaess[12], A. Blanco[70], J. Blazek[25], C. Bleve[50,43], M. Boháčová[25], D. Boncioli[40,d], C. Bonifazi[22], N. Borodai[67], A.M. Botti[8,33], J. Brack[83], I. Brancus[71], T. Bretz[35], A. Bridgeman[33], F.L. Briechle[35], P. Buchholz[37], A. Bueno[79], S. Buitink[63], M. Buscemi[52,42], K.S. Caballero-Mora[60], B. Caccianiga[44], L. Caccianiga[29], A. Cancio[11,8], F. Canfora[63], L. Caramete[72], R. Caruso[52,42], A. Castellina[48,47], G. Cataldi[43], L. Cazon[70], R. Cester[56,47], A.G. Chavez[61], A. Chiavassa[56,47], J.A. Chinellato[17], J. Chudoba[25], R.W. Clay[12], R. Colalillo[54,45], A. Coleman[91], L. Collica[47], M.R. Coluccia[50,43], R. Conceição[70], F. Contreras[9,10], M.J. Cooper[12], S. Coutu[91], C.E. Covault[81], J. Cronin[92], R. Dallier[e], S. D'Amico[49,43], B. Daniel[17], S. Dasso[5,3], K. Daumiller[33], B.R. Dawson[12], R.M. de Almeida[23], S.J. de Jong[63,65], G. De Mauro[63], J.R.T. de Mello Neto[22], I. De Mitri[50,43], J. de Oliveira[23], V. de Souza[15], J. Debatin[33], L. del Peral[78], O. Deligny[28], C. Di Giulio[55,46], A. Di Matteo[51,41], M.L. Díaz Castro[17], F. Diogo[70], C. Dobrigkeit[17], J.C. D'Olivo[62], A. Dorofeev[83], R.C. dos Anjos[21], M.T. Dova[4], A. Dundovic[36], J. Ebr[25], R. Engel[33], M. Erdmann[35], M. Erfani[37], C.O. Escobar[85,17], J. Espadanal[70], A. Etchegoyen[8,11], H. Falcke[63,66,65], K. Fang[92], G. Farrar[88], A.C. Fauth[17], N. Fazzini[85], B. Fick[87], J.M. Figueira[8], A. Filevich[8], A. Filipčič[75,76], O. Fratu[74], M.M. Freire[6], T. Fujii[92], A. Fuster[8,11], B. García[7], D. Garcia-Pinto[77], F. Gaté, H. Gemmeke[34], A. Gherghel-Lascu[71], P.L. Ghia[29], U. Giaccari[22], M. Giammarchi[44], M. Giller[68], D. Głas[69], C. Glaser[35], H. Glass[85], G. Golup[1], M. Gómez Berisso[1], P.F. Gómez Vitale[9,10], N. González[8,33], B. Gookin[83], J. Gordon[90], A. Gorgi[48,47], P. Gorham[93], P. Gouffon[16], A.F. Grillo[40], T.D. Grubb[12], F. Guarino[54,45], G.P. Guedes[18], M.R. Hampel[8,11], P. Hansen[4], D. Harari[1], T.A. Harrison[12], J.L. Harton[83], Q. Hasankiadeh[64], A. Haungs[33], T. Hebbeker[35], D. Heck[33], P. Heimann[37], A.E. Herve[32], G.C. Hill[12], C. Hojvat[85], E. Holt[33,8], P. Homola[67], J.R. Hörandel[63,65], P. Horvath[26], M. Hrabovský[26], T. Huege[33], J. Hulsman[8,33], A. Insolia[52,42], P.G. Isar[72], I. Jandt[31], S. Jansen[63,65], J.A. Johnsen[82], M. Josebachuili[8], A. Kääpä[31], O. Kambeitz[32], K.H. Kampert[31], P. Kasper[85], I. Katkov[32], B. Keilhauer[33], E. Kemp[17], R.M. Kieckhafer[87], H.O. Klages[33], M. Kleifges[34], J. Kleinfeller[9], R. Krause[35], N. Krohm[31], D. Kuempel[35], G. Kukec Mezek[76], N. Kunka[34], A. Kuotb Awad[33], D. LaHurd[81], L. Latronico[47], M. Lauscher[35], P. Lautridou, P. Lebrun[85], R. Legumina[68], M.A. Leigui de Oliveira[20], A. Letessier-Selvon[29], I. Lhenry-Yvon[28], K. Link[32], L. Lopes[70], R. López[57], A. López Casado[80], Q. Luce[28], A. Lucero[8,11], M. Malacari[12], M. Mallamaci[53,44], D. Mandat[25], P. Mantsch[85], A.G. Mariazzi[4], I.C. Mariş[79], G. Marsella[50,43], D. Martello[50,43], H. Martinez[58], O. Martínez Bravo[57], J.J. Masías Meza[3], H.J. Mathes[33], S. Mathys[31], J. Matthews[86], J.A.J. Matthews[95], G. Matthiae[55,46], E. Mayotte[31], P.O. Mazur[85], C. Medina[82], G. Medina-Tanco[62], D. Melo[8], A. Menshikov[34], S. Messina[64], M.I. Micheletti[6], L. Middendorf[35], I.A. Minaya[77], L. Miramonti[53,44], B. Mitrica[71], D. Mockler[32], L. Molina-Bueno[79], S. Mollerach[1], F. Montanet[30], C. Morello[48,47], M. Mostafá[91], G. Müller[35], M.A. Muller[17,19], S. Müller[33,8], I. Naranjo[1], S. Navas[79], L. Nellen[62], J. Neuser[31], P.H. Nguyen[12], M. Niculescu-Oglinzanu[71], M. Niechciol[37], L. Niemietz[31], T. Niggemann[35], D. Nitz[87], D. Nosek[27], V. Novotny[27], H. Nožka[26], L.A. Núñez[24], L. Ochilo[37], F. Oikonomou[91], A. Olinto[92], D. Pakk Selmi-Dei[17], M. Palatka[25], J. Pallotta[2], P. Papenbreer[31], G. Parente[80], A. Parra[57], T. Paul[89,84], M. Pech[25], F. Pedreira[80], J. Pękala[67], R. Pelayo[59], J. Peña-Rodriguez[24], L. A. S. Pereira[17], L. Perrone[50,43], C. Peters[35], S. Petrera[51,38,41], J. Phuntsok[91], R. Piegaia[3], T. Pierog[33], P. Pieroni[3], M. Pimenta[70], V. Pirronello[52,42], M. Platino[8], M. Plum[35], C. Porowski[67], R.R. Prado[15], P. Privitera[92], M. Prouza[25], E.J. Quel[2], S. Querchfeld[31], S. Quinn[81], R. Ramos-Pollant[24], J. Rautenberg[31], O. Ravel, D. Ravignani[8], D. Reinert[35], B. Revenu, J. Ridky[25], M. Risse[37], P. Ristori[2], V. Rizi[51,41], W. Rodrigues de Carvalho[80], G. Rodriguez Fernandez[55,46], J. Rodriguez Rojo[9], M.D. Rodríguez-Frías[78], D. Rogozin[33], J. Rosado[77], M. Roth[33], E. Roulet[1], A.C. Rovero[5], S.J. Saffi[12], A. Saftoiu[71], H. Salazar[57], A. Saleh[76], F. Salesa Greus[91], G. Salina[46], J.D. Sanabria Gomez[24], F. Sánchez[8], P. Sanchez-Lucas[79], E.M. Santos[16], E. Santos[8], F. Sarazin[82], B. Sarkar[31], R. Sarmento[70],

C. Sarmiento-Cano[8], R. Sato[9], C. Scarso[9], M. Schauer[31], V. Scherini[50,43], H. Schieler[33], D. Schmidt[33,8], O. Scholten[64,c], P. Schovánek[25], F.G. Schröder[33], A. Schulz[33], J. Schulz[63], J. Schumacher[35], S.J. Sciutto[4], A. Segreto[39,42], M. Settimo[29], A. Shadkam[86], R.C. Shellard[13], G. Sigl[36], G. Silli[8,33], O. Sima[73], A. Śmiałkowski[68], R. Šmída[33], G.R. Snow[94], P. Sommers[91], S. Sonntag[37], J. Sorokin[12], R. Squartini[9], D. Stanca[71], S. Stanič[76], J. Stasielak[67], F. Strafella[50,43], F. Suarez[8,11], M. Suarez Durán[24], T. Sudholz[12], T. Suomijärvi[28], A.D. Supanitsky[5], M.S. Sutherland[90], J. Swain[89], Z. Szadkowski[69], O.A. Taborda[1], A. Tapia[8], A. Tepe[37], V.M. Theodoro[17], C. Timmermans[65,63], C.J. Todero Peixoto[14], L. Tomankova[33], B. Tomé[70], A. Tonachini[56,47], G. Torralba Elipe[80], D. Torres Machado[22], M. Torri[53], P. Travnicek[25], M. Trini[76], R. Ulrich[33], M. Unger[88,33], M. Urban[35], A. Valbuena-Delgado[24], J.F. Valdés Galicia[62], I. Valiño[80], L. Valore[54,45], G. van Aar[63], P. van Bodegom[12], A.M. van den Berg[64], A. van Vliet[63], E. Varela[57], B. Vargas Cárdenas[62], G. Varner[93], J.R. Vázquez[77], R.A. Vázquez[80], D. Veberič[33], V. Verzi[46], J. Vicha[25], L. Villaseñor[61], S. Vorobiov[76], H. Wahlberg[4], O. Wainberg[8,11], D. Walz[35], A.A. Watson[a], M. Weber[34], A. Weindl[33], L. Wiencke[82], H. Wilczyński[67], T. Winchen[31], D. Wittkowski[31], B. Wundheiler[8], S. Wykes[63], L. Yang[76], D. Yelos[11,8], A. Yushkov[8], E. Zas[80], D. Zavrtanik[76,75], M. Zavrtanik[75,76], A. Zepeda[58], B. Zimmermann[34], M. Ziolkowski[37], Z. Zong[28], F. Zuccarello[52,42]

[1] Centro Atómico Bariloche and Instituto Balseiro (CNEA-UNCuyo-CONICET), Argentina
[2] Centro de Investigaciones en Láseres y Aplicaciones, CITEDEF and CONICET, Argentina
[3] Departamento de Física and Departamento de Ciencias de la Atmósfera y los Océanos, FCEyN, Universidad de Buenos Aires, Argentina
[4] IFLP, Universidad Nacional de La Plata and CONICET, Argentina
[5] Instituto de Astronomía y Física del Espacio (IAFE, CONICET-UBA), Argentina
[6] Instituto de Física de Rosario (IFIR) – CONICET/U.N.R. and Facultad de Ciencias Bioquímicas y Farmacéuticas U.N.R., Argentina
[7] Instituto de Tecnologías en Detección y Astropartículas (CNEA, CONICET, UNSAM) and Universidad Tecnológica Nacional – Facultad Regional Mendoza (CONICET/CNEA), Argentina
[8] Instituto de Tecnologías en Detección y Astropartículas (CNEA, CONICET, UNSAM), Centro Atómico Constituyentes, Comisión Nacional de Energía Atómica, Argentina
[9] Observatorio Pierre Auger, Argentina
[10] Observatorio Pierre Auger and Comisión Nacional de Energía Atómica, Argentina
[11] Universidad Tecnológica Nacional – Facultad Regional Buenos Aires, Argentina
[12] University of Adelaide, Australia
[13] Centro Brasileiro de Pesquisas Fisicas (CBPF), Brazil
[14] Universidade de São Paulo, Escola de Engenharia de Lorena, Brazil
[15] Universidade de São Paulo, Inst. de Física de São Carlos, São Carlos, Brazil
[16] Universidade de São Paulo, Inst. de Física, São Paulo, Brazil
[17] Universidade Estadual de Campinas (UNICAMP), Brazil
[18] Universidade Estadual de Feira de Santana (UEFS), Brazil
[19] Universidade Federal de Pelotas, Brazil
[20] Universidade Federal do ABC (UFABC), Brazil
[21] Universidade Federal do Paraná, Setor Palotina, Brazil
[22] Universidade Federal do Rio de Janeiro (UFRJ), Instituto de Física, Brazil
[23] Universidade Federal Fluminense, Brazil
[24] Universidad Industrial de Santander, Colombia
[25] Institute of Physics (FZU) of the Academy of Sciences of the Czech Republic, Czech Republic
[26] Palacky University, RCPTM, Czech Republic
[27] University Prague, Institute of Particle and Nuclear Physics, Czech Republic
[28] Institut de Physique Nucléaire d'Orsay (IPNO), Université Paris 11, CNRS-IN2P3, France
[29] Laboratoire de Physique Nucléaire et de Hautes Energies (LPNHE), Universités Paris 6 et Paris 7, CNRS-IN2P3, France

[30] Laboratoire de Physique Subatomique et de Cosmologie (LPSC), Université Grenoble-Alpes, CNRS/IN2P3, France
[31] Bergische Universität Wuppertal, Department of Physics, Germany
[32] Karlsruhe Institute of Technology, Institut für Experimentelle Kernphysik (IEKP), Germany
[33] Karlsruhe Institute of Technology, Institut für Kernphysik (IKP), Germany
[34] Karlsruhe Institute of Technology, Institut für Prozessdatenverarbeitung und Elektronik (IPE), Germany
[35] RWTH Aachen University, III. Physikalisches Institut A, Germany
[36] Universität Hamburg, II. Institut für Theoretische Physik, Germany
[37] Universität Siegen, Fachbereich 7 Physik – Experimentelle Teilchenphysik, Germany
[38] Gran Sasso Science Institute (INFN), L'Aquila, Italy
[39] INAF – Istituto di Astrofisica Spaziale e Fisica Cosmica di Palermo, Italy
[40] INFN Laboratori Nazionali del Gran Sasso, Italy
[41] INFN, Gruppo Collegato dell'Aquila, Italy
[42] INFN, Sezione di Catania, Italy
[43] INFN, Sezione di Lecce, Italy
[44] INFN, Sezione di Milano, Italy
[45] INFN, Sezione di Napoli, Italy
[46] INFN, Sezione di Roma "Tor Vergata", Italy
[47] INFN, Sezione di Torino, Italy
[48] Osservatorio Astrofisico di Torino (INAF), Torino, Italy
[49] Università del Salento, Dipartimento di Ingegneria, Italy
[50] Università del Salento, Dipartimento di Matematica e Fisica "E. De Giorgi", Italy
[51] Università dell'Aquila, Dipartimento di Scienze Fisiche e Chimiche, Italy
[52] Università di Catania, Dipartimento di Fisica e Astronomia, Italy
[53] Università di Milano, Dipartimento di Fisica, Italy
[54] Università di Napoli "Federico II", Dipartimento di Fisica "Ettore Pancini", Italy
[55] Università di Roma "Tor Vergata", Dipartimento di Fisica, Italy
[56] Università Torino, Dipartimento di Fisica, Italy
[57] Benemérita Universidad Autónoma de Puebla (BUAP), México
[58] Centro de Investigación y de Estudios Avanzados del IPN (CINVESTAV), México
[59] Unidad Profesional Interdisciplinaria en Ingeniería y Tecnologías Avanzadas del Instituto Politécnico Nacional (UPIITA-IPN), México
[60] Universidad Autónoma de Chiapas, México
[61] Universidad Michoacana de San Nicolás de Hidalgo, México
[62] Universidad Nacional Autónoma de México, México
[63] Institute for Mathematics, Astrophysics and Particle Physics (IMAPP), Radboud Universiteit, Nijmegen, Netherlands
[64] KVI – Center for Advanced Radiation Technology, University of Groningen, Netherlands
[65] Nationaal Instituut voor Kernfysica en Hoge Energie Fysica (NIKHEF), Netherlands
[66] Stichting Astronomisch Onderzoek in Nederland (ASTRON), Dwingeloo, Netherlands
[67] Institute of Nuclear Physics PAN, Poland
[68] University of Łódź, Faculty of Astrophysics, Poland
[69] University of Łódź, Faculty of High-Energy Astrophysics, Poland
[70] Laboratório de Instrumentação e Física Experimental de Partículas – LIP and Instituto Superior Técnico – IST, Universidade de Lisboa – UL, Portugal
[71] "Horia Hulubei" National Institute for Physics and Nuclear Engineering, Romania
[72] Institute of Space Science, Romania
[73] University of Bucharest, Physics Department, Romania

[74] University Politehnica of Bucharest, Romania
[75] Experimental Particle Physics Department, J. Stefan Institute, Slovenia
[76] Laboratory for Astroparticle Physics, University of Nova Gorica, Slovenia
[77] Universidad Complutense de Madrid, Spain
[78] Universidad de Alcalá de Henares, Spain
[79] Universidad de Granada and C.A.F.P.E., Spain
[80] Universidad de Santiago de Compostela, Spain
[81] Case Western Reserve University, USA
[82] Colorado School of Mines, USA
[83] Colorado State University, USA
[84] Department of Physics and Astronomy, Lehman College, City University of New York, USA
[85] Fermi National Accelerator Laboratory, USA
[86] Louisiana State University, USA
[87] Michigan Technological University, USA
[88] New York University, USA
[89] Northeastern University, USA
[90] Ohio State University, USA
[91] Pennsylvania State University, USA
[92] University of Chicago, USA
[93] University of Hawaii, USA
[94] University of Nebraska, USA
[95] University of New Mexico, USA
[a] School of Physics and Astronomy, University of Leeds, Leeds, United Kingdom
[b] Max-Planck-Institut für Radioastronomie, Bonn, Germany
[c] also at Vrije Universiteit Brussels, Brussels, Belgium
[d] now at Deutsches Elektronen-Synchrotron (DESY), Zeuthen, Germany
[e] SUBATECH, École des Mines de Nantes, CNRS-IN2P3, Université de Nantes